The kinetics of the low-pressure chemical vapor deposition of polycrystalline silicon from silane

The Kinetics of the Low-Pressure Chemical Vapor Deposition of Polycrystalline Silicon from Silane

W. L. M. Weerts,[a] M. H. J. M. de Croon, and G. B. Marin[b]

Laboratorium voor Chemische Technologie, Eindhoven University of Technology, 5600 MB Eindhoven, The Netherlands

ABSTRACT

The kinetics of the deposition of polycrystalline silicon from silane were studied at 25–125 Pa and 863–963 K using a continuous flow perfectly mixed reactor equipped with a microbalance and a quadrupole mass spectrometer for in situ deposition rate measurements and on-line gas-phase analysis. It was possible to obtain rate coefficients that are intrinsic, i.e., only determined by chemical phenomena. A four-step elementary gas-phase reaction network coupled to a ten-step elementary surface network was able to describe the experimental data. Pressure falloff behavior of gas-phase reactions was taken into account using the Rice–Ramsberger–Kassel–Marcus theory. In the surface reaction mechanism, adsorption of silane, hydrogen, and highly reactive gas-phase intermediates and first-order desorption of hydrogen are the only kinetically significant steps. Silylene and disilane are the most abundant gas-phase intermediates, causing typically one fifth of the overall silicon growth.

Introduction

The kinetics of the low-pressure chemical vapor deposition (LPCVD) of polycrystalline silicon from silane has been the subject of a number of experimental studies carried out in conventional hotwall multiwafer LPCVD reactors.[1-5] Although the general trends observed in this type of reactors may be correlated with the chemistry and kinetics, the interpretation of these investigations is not straightforward, because the growth rate is determined both by transport phenomena and intrinsic kinetics. Another shortcoming is that the growth rates are only determined at the end of a run and are quantitatively linked with the process conditions such as inlet composition and flow rates without taking into account the actual gas-phase composition at the position where deposition occurs. The present study, however, reports on steady-state experiments on polycrystalline silicon deposition from silane in a microbalance reactor setup. This reactor allows a direct measurement of the growth rate combined with an on-line analysis of the corresponding gas-phase composition.[6,7] In spite of irreducible transport limitations it is possible to obtain intrinsic kinetic data with this experimental setup. It requires the analysis of the obtained data with a reactor model that takes into account the transport limitations in an appropriate way. The latter features only binary diffusion coefficients, which can be calculated independently, as transport parameters.

Based on the experiments a kinetic model for polycrystalline silicon deposition is developed that is valid over a wide range of experimental conditions. This model consists of four elementary gas-phase reactions coupled to ten elementary reactions taking place on the growing silicon surface. The gas-phase reaction network is constructed as a closed subsystem among species that are thermodynamically favored and consists of reactions that are unimolecular in at least one direction. To describe the effects of pressure adequately, the falloff behavior of each of the unimolecular rate coefficients is quantified using the Rice–Ramsberger–Kassel–Marcus (RRKM) theory.[8]

The surface reaction network is based on recent mechanistic studies of silane chemisorption on well-defined single-crystal silicon surfaces using temperature-programmed desorption (TPD) combined with static secondary ion mass spectrometry (SSIMS),[9-13] laser-induced thermal desorption (LITD),[14,15] scanning tunneling microscopy (STM),[16,17] and modulated molecular beam scattering (MMBS).[18] It consists of a six-step elementary reaction mechanism for the deposition of silicon from silane, supplemented with elementary adsorption reactions for the silicon-containing species formed through the gas-phase reactions.

The developed kinetic model provides insight in the relative importance of the gas-phase reactions in the polycrystalline silicon deposition process. It can also be used to predict the influence of various process variables on the performance of an industrial hotwall multiwafer LPCVD reactor as is shown by Weerts[7] and by Weerts et al.[19,20]

Experimental

Equipment and procedures.—Silane (ultrapure quality) was used as the main reactant gas. Hydrogen (quality 6.0) was fed to study inhibition effects on the gas-phase and surface kinetics. Argon was used both as inert diluent gas and as internal standard for quantitative analysis of the gas-phase composition with a quadrupole mass spectrometer. The flow rates of these process gases were established with mass flow controllers and ranged typically between 3 and 30 sccm, corresponding to mean residence times between 0.1 and 1 s.

After premixing, the feed mixture was preheated to reduce intrareactor temperature gradients and injected through the four nozzles of a cross-shaped injector located in the middle of a quartz spherical reactor. Just above the injector, a 10 × 15 mm silicon sample was suspended from a microbalance. The silicon sample was cleaved from a double-side polished (100) p-type wafer with a resistivity of ~0.035 Ω cm and an average thickness of 410 μm. The reactor was heated externally using an electrical resistance oven. Temperature regulation was performed on the basis of a Chromel-Alumel thermocouple located between the oven and the reactor wall. The reaction temperature was measured with a second Chromel-Alumel thermocouple inside a thermowell located near the silicon sample in the center of the reactor. Vacuum was maintained by a dual-stage rotary-vane mechanical pump. The reactor pressure was regulated via the exhaust rate of effluent gases independent of upstream gas flow rates. This was accomplished with the so-called gas ballast or gas bypass technique, which involves the injection of nitrogen into the pump throat, thereby forcing the total pressure to the required value. Prior to each series of experiments the silicon sample and reactor wall were precoated with polycrystalline silicon at 50 Pa and 900 K for 30 min after pretreatment with hydrogen at 900 K for 10 min. Further details are given by Weerts et al.[6,7]

The weight increase due to silicon deposition on the 10 × 15 mm sample in the middle of the reactor was measured with a microbalance (Cahn D-200), which was operated in the weight range from 0 to 2 mg with a resolution of 0.1 μg under ideal circumstances. Calibration was performed prior to each series of experiments.

Quantitative analysis of silane and Si_2H_x, the latter denoting the total of disilane (Si_2H_6), silylsilylene (H_3SiSiH), and disilene (H_2SiSiH_2), was performed by directing a fraction of the reactor effluent through an orifice inlet to a differentially pumped quadrupole mass spectrometer (Fisons SXP Elite 300H), which was operated at a constant ion-

[a] Present address: Philips CFT, Eindhoven, The Netherlands.
[b] Present address: Laboratorium voor Petrochemische Techniek, Universiteit Gent, Ghent, Belgium.

ization energy of 70 eV. The detection limit of the quadrupole mass spectrometer (QMS) was about 1 ppm, whereas its mass resolution, defined as the full width at half height, amounted to 0.5 amu.

Separate quantitative analysis of disilane, silylsilylene, and disilene was impossible, because the latter two dimers cannot be calibrated in pure form due to their high reactivity. In addition, the fragmentation patterns of silylsilylene and disilene probably completely overlap with each other and with that of disilane, making discrimination between these silicon dimers very difficult. Quantitative analysis of hydrogen was considered not accurate enough due to the rather low pumping efficiency for this component. The outlet molar flow rate of hydrogen was calculated from a hydrogen mass balance over the reactor.

During the calibration prior to each series of experiments, the relative sensitivity factors of silane and Si_2H_x were determined with respect to the internal standard argon. For this purpose an SiH_4–Si_2H_6–Ar mixture was used. In this way it was implicitly assumed that silylsilylene and disilene possess the same QMS sensitivity as disilane. This assumption is supported by the fact that silylsilylene and disilene are both primary QMS fragmentation products of disilane. Deviations of the QMS sensitivities of silylsilylene and disilene from the QMS sensitivity of disilane would probably have no large effect on the final results. From kinetic/reactor modeling studies reported in literature, it is known that during silicon deposition at low total pressures silylsilylene and disilene are present in the gas phase in only small amounts compared to disilane.[21,22]

A total of 250 kinetic experiments was performed over the range of experimental conditions listed in Table I. This range coincides with the industrially relevant operating conditions for the deposition of polycrystalline silicon from silane in a conventional hotwall multiwafer LPCVD reactor. The structure and purity of the deposited layers were studied using scanning electron microscopy (SEM) and Auger electron spectroscopy (AES). Polycrystalline silicon with a columnar structure was deposited. AES measurements combined with depth profiling revealed the presence of small amounts of oxygen and carbon in about the five topmost layers of single deposited silicon layers. Other contaminants were not detected.

The inlet molar flow rates were measured with the mass flow controllers; the outlet molar flow rates were derived from the mass spectrometric data. The silicon growth rate was determined by linear regression of the measured mass vs. time curve. The quality of the experimental data was verified by means of a silicon balance between reactor inlet stream and reactor outlet stream plus growth rate. The total deposition surface area was calculated from the geometric surface areas of both silicon sample and reactor wall and amounted typically to 1.45×10^{-2} m^2. Experiments with a silicon mass balance which deviated more than 5% were rejected.

Parameter estimation.—The kinetic and thermodynamic parameters of the reaction network were estimated using the single- or multiresponse Marquardt algorithm for nonlinear regression.[23] Single-response regression was used for the regression of the experimental deposition rates in the absence of gas-phase reactions to estimate kinetic and thermodynamic parameters. In order to facilitate the simultaneous estimation of a standard activation entropy and enthalpy or of a standard entropy and enthalpy difference, reparameterization was applied[24] based on an average temperature of the experiments of 915.5 K. In total, the silicon growth rates from 150 experiments, covering the range of experimental conditions listed in the second column of Table I, were used as responses during the regression. Multiresponse regression was used for the regression of the experimental data in the presence of gas-phase reactions, i.e., of the silicon deposition rate and of the outlet molar flow rates of silane and Si_2H_x. Calculated responses were obtained by solving numerically the continuity equations for gas-phase and surface components and for solid silicon as described by Weerts et al.[6] The calculated Si_2H_x response was obtained by summing the individually calculated outlet molar flow rates of H_3SiSiH, H_2SiSiH_2, and Si_2H_6. In order to facilitate the parameter estimation, reparameterization was again applied based on an average temperature of the experiments of 914.8 K. A total of 210 experiments, covering the complementary ranges of experimental conditions listed in the second and third column of Table I, were used during the regression. Si_2H_x responses from experiments at total pressures lower than 50 Pa were not considered, because gas-phase reactions were found to be insignificant at these pressures. Hence, the total number of experimental Si_2H_x responses considered during the regression amounted to 60.

Model discrimination was based on statistical significance of the individual parameter estimates as well as of the global regression. The parameter estimates were tested for significance by means of their approximate individual t values. The approximate individual t values were used to determine the two-sided 95% confidence intervals. The significance of the global regression was expressed by means of the ratio of the mean regression sum of squares to the mean residual sum of squares, which is distributed according to F.[25] Discrimination among rival models was based upon statistical testing, whenever it was impossible by direct process observation or physicochemical laws.

Table I. Experimental conditions covered during the regression analysis.

	Without gas-phase reactions	With gas-phase reactions
P_t (Pa)	25–50	50–125
T (K)	863–963	887–963
$V/F_{SiH_4,0}$ (m^3 s mol^{-1})	22–91	11–55
X_{SiH_4} (%)	0.4–64	1.6–59
$H_2/SiH_4\|_0$	0–2	1.0
$SiH_4/Ar\|_0$	0.7–9	4.5

Effects of Process Conditions

Space time.—Figure 1 shows the silicon growth rate as a function of silane conversion at 50 Pa and different temperatures. The increase in silane conversion was brought about by an increase in silane space time, i.e., of the ratio of reactor volume and inlet molar flow rate of silane. The space-time concept here should not be confused with the residence time. Residence time in a continuously stirred tank reactor (CSTR) is the ratio of reactor volume and volumetric flow rate at the outlet of the reactor. Because of mole production and/or consumption in homogeneous and heterogeneous reactions in the $SiH_4/H_2/Si$ system, the outlet volumetric flow rate is not equal to the inlet volumetric flow rate. Thus, the residence time in this case is rather ill-defined. Space time as used here is a time scale at inlet conditions equal to the ratio of the residence time, calculated from the inlet volumetric flow rate, and the inlet concentration of silane. Only under zero conversion conditions are residence time and space time proportional to each other. Independence of production rate on the silane conversion corresponds to a so-called differential reactor operation with respect to that reaction.[26] At 50 Pa the laboratory reactor satisfies differential operation with respect to silicon deposition up to roughly 912 K in case pure silane is fed. Comparison of similar sets of growth rate vs. conversion data at different total pressures and temperatures while cofeeding hydrogen revealed that addition of hydrogen expands the differential regime toward higher pressures and temperatures.

The deviation from differential operation can be attributed to the occurrence of gas-phase reactions, as evidenced by Fig. 2 showing the effect of silane space time on the normalized Si_2H_x concentration at 912 K and different total pressures. Except for 50 Pa, a maximum in the normalized Si_2H_x concentration is observed at each pressure. The maxima are attained at short space times. With

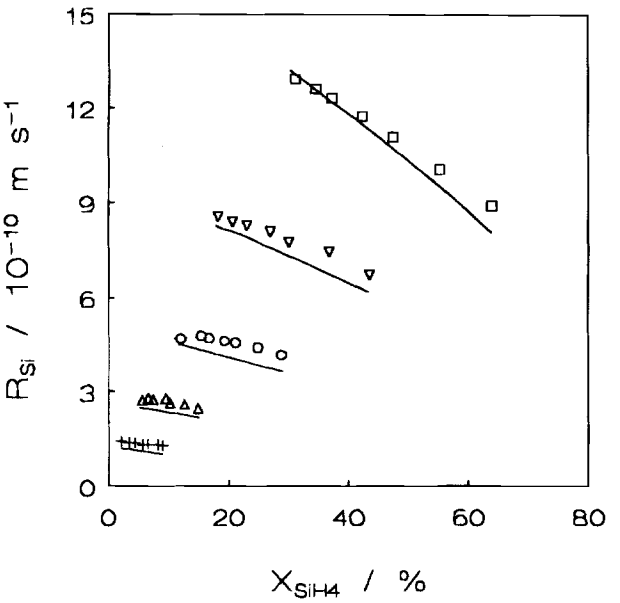

Fig. 1. Silicon growth rate vs. silane conversion. Lines: calculated using the reactor model equations of Weerts et al.[6] and the gas-phase and surface reactions listed in Tables II and III with corresponding parameter values given in Tables II and V. Points: experiments. Conditions: $SiH_4/Ar|_0$ = 4.0, P_t = 50 Pa; and T = (+) 863, (△) 888, (○) 912, (▽) 938, and (□) 963 K.

increasing total pressure the maximum Si_2H_x concentration increases proportionally to the second power of the total pressure without a change in the corresponding space time. This dependence can be explained on the basis of a parallel, consecutive kinetic scheme accounting for silicon deposition from silane and from disilane (Si_2H_x), the latter produced through pyrolysis of silane, coupled to a perfectly stirred tank reactor model.[6,7] The occurrence of gas-phase reactions above roughly 50 Pa at 912 K is in good agreement with the results of Holleman and Verweij,[5] who studied the kinetics of silicon deposition in a conventional hotwall multiwafer LPCVD reactor. The measured silicon growth rates appeared to be independent of interwafer spacing, i.e., of the volume-to-surface ratio, up to total pressures of 60 Pa while feeding pure silane at 900 K, indicating the insignificance of gas-phase reactions at lower pressures. The amount of Si_2H_x components measured in the gas phase varies between 0.1 and 1 mol %. van den Brekel and Bollen[1] measured a typical ratio of 10^5:10^2:1 between monosilane, disilane, and trisilane at the outlet of a conventional LPCVD reactor. Although the observed Si_2H_x molar fractions are in good agreement with the ratio found by these authors, Si_3H_x components were not detected in the laboratory reactor. The amounts of these components obviously were too small to fall within the detection limit of the QMS, i.e., 1 ppm.

Pressure.—In the pressure range from 25 to 50 Pa gas-phase reactions are not important and silicon deposition is predominantly determined by heterogeneous decomposition of silane. The experimental data reveal an increasing silicon growth rate with increasing inlet partial pressure of silane. Depending on silane space time and feed composition, partial reaction orders between 0.28 and 0.44 are obtained at 912 K.

At typical LPCVD conditions, Claassen et al.[2] and Hitchman et al.[27] report growth rates that are linear in silane pressure, whereas the data of van den Brekel and Bollen[1] reveal a less than linear dependence. Holleman and Aarnink[28] report growth rates that are proportional to the square root of the silane partial pressure. Farrow[29] observed a linear dependence of the silicon growth rate on silane partial pressure over a temperature range from 293 to 1473 K and silane pressures ranging from 1×10^{-3} to 133 Pa. This dependence is supported by later work of Henderson and Helm,[30] Duchemin et al.,[31] and Farnaam and Olander.[18]

Compared to the pressure effect on the silicon growth rate in the differential regime, i.e., at pressures up to 50 Pa, a more pronounced effect is observed in the regime where gas-phase reactions are important. This effect is strongest at the shorter space times where larger amounts of Si_2H_x and other reactive intermediates are present in the gas phase (see Fig. 2). Figure 3 shows the silicon growth rate, the silane conversion, and the Si_2H_x selectivity, defined as the ratio of the number of moles of silicon atoms in Si_2H_x formed to the total number of moles of silicon atoms in silane converted, vs. the silane space time at 100 Pa and 963 K. The

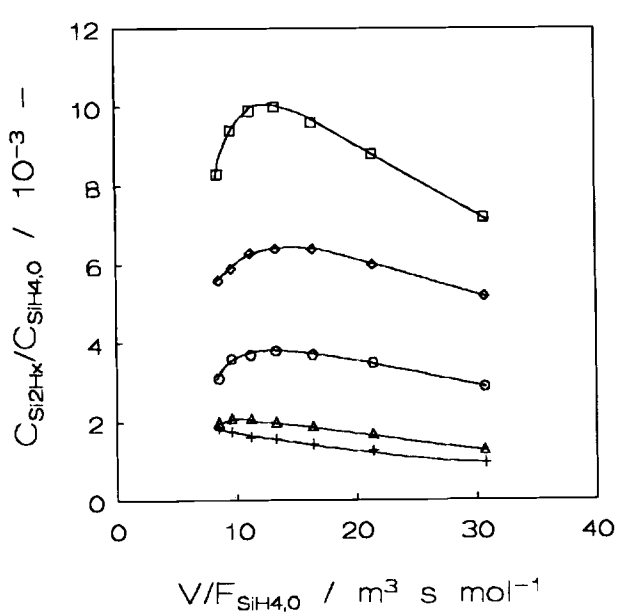

Fig. 2. Normalized Si_2H_x concentration vs. silane space time. $SiH_4/Ar|_0$ = 4.0; T = 912 K. + P_t = 50 Pa; and (△) P_t = 60, (○) P_t = 80, (◇) P_t = 100, and (□) P_t = 125 Pa.

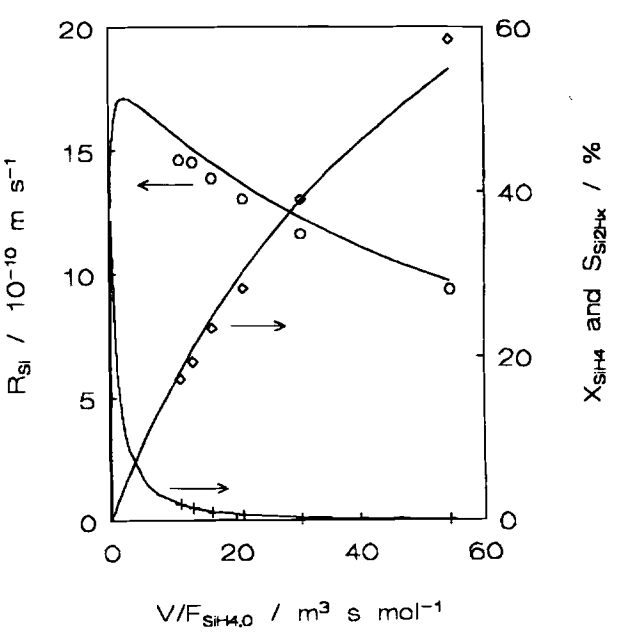

Fig. 3. Silicon growth rate (○), silane conversion (◇), and Si_2H_x selectivity (+) vs. silane space time. Lines: calculated using the reactor model equations of Weerts et al.[6] and the gas-phase and surface reactions listed in Tables II and III with corresponding parameter values given in Tables II and V. Points: experiments. Conditions: $SiH_4/Ar|_0$ = 4.5, $SiH_4/H_2|_0$ = 1.0, P_t = 100 Pa, T = 963 K.

experimentally observed growth rate indeed exhibits a maximum value at short space time. The Si_2H_x selectivity generally decreases with increasing silane conversion.

Inlet hydrogen-to-silane ratio.—Figure 4 shows the effect of the inlet hydrogen-to-silane ratio on the silicon growth rate at 912 K and total pressures of 25 and 50 Pa. The use of the inlet hydrogen-to-silane ratio instead of the actually prevailing one is justified, because the laboratory reactor is operated differentially at the conditions considered. Changing a 1:2 into a 5:4 H_2/SiH_4 feed ratio reduces the silicon growth rate by approximately 15%. Due to hydrogen adsorption the fraction of vacant surface sites is reduced and silane adsorption is hampered. As a result, the silicon growth rate drops. At 25 Pa hydrogen inhibition is slightly more pronounced than at 50 Pa.

Apparently conflicting reports concerning the existence of a hydrogen effect are found in the literature. Henderson and Helm,[30] van den Brekel and Bollen,[1] Buss et al.,[32] Robbins and Young,[33] and Foster et al.[34] report no evidence for hydrogen inhibition. Holleman[35] reports growth rates that are inversely proportional to the hydrogen partial pressure at 898 K. According to the same author the hydrogen inhibiting effect becomes weaker at higher temperatures and turns into an inverse square root dependence at 973 K. Hottier and Cadoret[36] observed an inverse proportional dependence, whereas experiments of Duchemin et al.[31] with silane partial pressures upto 26 Pa and temperatures upto 1263 K again are in support of the inverse square root dependence on hydrogen pressure. It should be noted that in those cases where hydrogen inhibiting effects were reported to be absent, in general no large excesses of hydrogen were used.

Temperature.—Figure 5 shows the silane conversion as a function of space time over a broad range of temperatures at 50 Pa. With increasing temperature the silane conversion considerably increases, reaching values as high as 60% at 963 K. The experiments also show the existence of a differential operating regime with respect to silane conversion at the lower temperatures considered.

Figure 1 already showed that at a given silane conversion the silicon growth rate considerably increases with

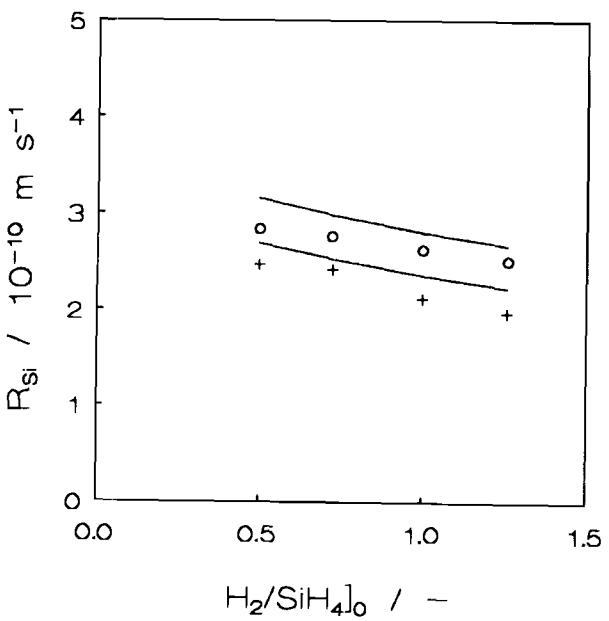

Fig. 4. Silicon growth rate vs. inlet hydrogen-to-silane ratio. Lines: calculated using the reactor model equations of Weerts et al.[6] and the gas-phase and surface reactions listed in Tables II and III with corresponding parameter values given in Tables II and V. Points: experiments. Conditions: T = 912 K, $F_{SiH_4,0} = 2.6 \times 10^{-6}$ mol s^{-1}, $F_0 = 6.3 \times 10^{-6}$ mol s^{-1}, argon as balance: (+) P_t = 25 Pa, (○) P_t = 50 Pa.

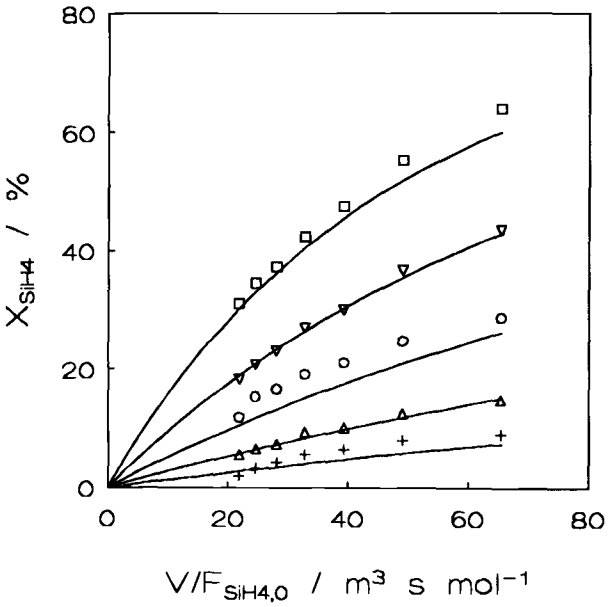

Fig. 5. Silane conversion vs. silane space time. Lines: calculated using the reactor model equations of Weerts et al.[6] and the gas-phase and surface reactions listed in Tables II and III with corresponding parameter values given in Tables II and V. Points: experiments. Conditions: $SiH_4/Ar]_0$ = 4.0, P_t = 50 Pa: T = (+) 863, (△) 888, (○) 912, (▽) 938, and (□) 963 K.

increasing temperature. The apparent activation energy obtained from the least mean squares slope of an Arrhenius plot in the temperature range from 863 to 963 K at 50 Pa amounts to 155.5 kJ mol^{-1}. Apparent activation energies for silicon deposition at LPCVD conditions range from 130 to 180 kJ mol^{-1}.[1,2,35-38]

Network Construction

Gas-phase reactions.—In principle it is possible to construct a gas-phase reaction network that consists of a very large number of reactions (see, e.g., Becerra and Walsh[22]; Ring and O'Neal[39]), but in this study the network was purposely limited to a minimal set of reactions. In the range of experimental conditions covered during the kinetic experiments, i.e., temperatures between 863 and 963 K and total pressures between 25 and 100 Pa, seven gas-phase species have an equilibrium molar fraction larger than 1×10^{-5}, i.e., SiH_4, Si_2H_6, H_2SiSiH_2, Si_2H_2, Si_3H_8, Si_3, and H_2. The lower limit of 1×10^{-5} reflects a minimum contribution to the silicon deposition rate of 1% compared to that of silane, assuming unit reaction probabilities for the homogeneously formed silicon-containing species and a value of 2×10^{-3} for silane.

Although Si_3 is an important species from a thermodynamic viewpoint, its formation rate is very slow and hence its kinetic significance can be neglected. In addition, the absence of trisilane and other Si_3H_x species in the reaction mixture provides direct evidence for the insignificance of chemical routes toward these species at the experimental conditions applied. Although SiH_2 is not important in a thermodynamic sense, it plays a key role in the overall gas-phase chemistry. It is formed in the initial silane decomposition reaction[40,41] and easily inserts into silane to form disilane.[42-45] Because H_2SiSiH_2 is formed by isomerization of H_3SiSiH,[46,47] one of the products of disilane decomposition,[48] this species needs to be considered as well. Inclusion of Si_2H_2, which in turn is formed from H_2SiSiH_2,[49,50] does not basically change the growth rate contribution along the homogeneous path, as both species are assumed to have unit reaction probabilities.[49,51] Hence, Si_2H_2 is omitted from the gas-phase kinetic scheme.

Based on these considerations the following set of silicon-containing species was considered in the gas-phase reaction network: SiH_4, SiH_2, Si_2H_6, H_3SiSiH, and H_2SiSiH_2.

Table II. Elementary reactions considered in the gas-phase (Eq. 1–4), and corresponding values for the pressure falloff correction constants (Eq. 12) based on RRKM calculations.

Reaction[a]	B_1	B_2 (J mol^{-1})	B_3 (J mol^{-1})
(r1) $SiH_4 \rightleftarrows SiH_2 + H_2$	1.0013	-3.55×10^1	1.23×10^1
(r2) $SiH_4 + SiH_2 \rightleftarrows Si_2H_6$	1.0953	1.21×10^3	1.80×10^2
(r3) $Si_2H_6 \rightleftarrows H_3SiSiH + H_2$	1.1076	1.97×10^3	1.55×10^2
(r4) $H_3SiSiH \rightleftarrows H_2SiSiH_2$	1.0001	7.86×10^{-2}	8.37×10^{-2}

[a] Pressure correction constants listed apply to the forward steps of reactions (r1), (r3), and (r4) and to the backward step of reaction (r2).

The corresponding elementary gas-phase reactions used to simulate the kinetic experiments are given in Table II. Note that only silicon hydride species containing an even number of hydrogen atoms are involved in the gas-phase kinetic scheme. The fact that the gas-phase chemistry of silane is determined merely by this kind of species is consistent with the gas-phase reaction networks recently published to describe the silicon deposition process at similar temperatures and total pressures ranging from 50 Pa to atmospheric pressure.[5,21,22,39,41,49-54]

Surface reactions.—The minimal set of elementary steps on the silicon surface considered in the kinetic model is shown in Table III. This way of presenting a complex reaction network was developed by Temkin[55] and allows a straightforward calculation of the net production rates of the components involved in the surface reactions. For a recent comprehensive treatise on the surface chemistry of Si, see the review of Waltenburg and Yates.[56]

It is known that hydrogen desorption, whether second order as on Si(111)–(7 × 7) [57-59] or first order as on Si(100)–(2 × 1), [14,15,59,60] is potentially slower than the chemisorption of SiH_4 and of homogeneously formed gas-phase intermediates, and subsequent surface reactions of silicon hydride species. Consequently, hydrogen adatoms are the only kinetically significant surface species. In the present work hydrogen desorption is accounted for via first-order kinetics, which is in line with the work reported by Holleman and Verweij.[5] These authors found good agreement between calculated and measured growth rates assuming first-order hydrogen desorption kinetics. The origin of the unusual first-order desorption kinetics as proposed for Si(100) is still a matter of debate in the literature. Wise et al.[59] attributed this first-order dependence to preferential pairing of the hydrogen adatoms on the silicon dimers of the Si(100)–(2 × 1) surface, leading to pairwise desorption. In the present work, however, a choice is made for the band model of Sinniah et al.,[14,15] which is another mechanism encountered for hydrogen desorption from Si(100)–(2 × 1). By using the latter model for hydrogen desorption, significantly better statistics were obtained in the description of the experimental data than by using the former. More elaborate models for hydrogen desorption from Si(100)–(2 × 1) exist in literature. For an overview on this matter see, e.g., the review by Doren.[61] Considering noncomplete pairing of hydrogen adatoms in the pairwise desorption mechanism necessitates the introduction of extra parameters into the kinetic analysis; however, this is not justifiable on statistical grounds with the present data. Sinniah et al.[14,15] measured first-order desorption kinetics with an apparent activation energy of 188 ± 8 kJ mol^{-1} and postulated the two-step mechanistic model illustrated by reactions (r13) and (r14) of Table III. The activated desorption proceeds via excitation of a covalently bound hydrogen adatom from a localized Si–H bond, denoted by H*, to a two-dimensional delocalized state H^e, reaction (r13). The symbol * denotes a dangling bond on a vacant silicon surface atom. The H^e state is bound to the surface by 188 kJ mol^{-1}, i.e., 188 kJ mol^{-1} higher in energy than the original Si–H bond possessing a bond strength of 376 kJ mol^{-1}. The final elementary step in the associative desorption is the reaction of the excited delocalized hydrogen atom, H^e, with a localized hydrogen adatom, H*, leading to H_2 desorption, reaction (r14). This reaction is considered to proceed potentially fast compared to the excitation of a hydrogen adatom, reaction (r13), giving rise to the first-order desorption kinetics. Furthermore, the formation of a localized hydrogen adatom via interaction of a delocalized hydrogen atom with a vacant surface site is considered very slow. For any appreciable coverage of localized hydrogen adatoms, the diffusion length of a H^e atom necessary to find such a localized hydrogen adatom is not very large, making recombination with another localized hydrogen adatom, reaction (r14), much more likely to occur than interaction with a vacant surface site, the reverse of reaction (r13). In order to take into account the hydrogen inhibition effects shown previously, dissociative adsorption of molecular hydrogen was considered by taking reaction (r14) reversible.

Table III. Elementary reactions considered on the silicon surface (r5–r14) with corresponding global adsorption reactions (α–ϵ) and global deposition paths (αα–ϵϵ).

	σ_α	σ_β	σ_γ	σ_δ	σ_ϵ	
$SiH_4 + 2^* \rightarrow SiH_3^* + H^*$	1	0	0	0	0	(r5)
$SiH_2 + {}^* \rightarrow SiH_2^*$	0	1	0	0	0	(r6)
$Si_2H_6 + {}^* \rightarrow SiH_4 + SiH_2^*$	0	0	1	0	0	(r7)
$H_3SiSiH + 2^* \rightarrow 2SiH_2^*$	0	0	0	1	0	(r8)
$H_2SiSiH_2 + 2^* \rightarrow 2SiH_2^*$	0	0	0	0	1	(r9)
$SiH_2^* + {}^* \rightarrow SiH_2^* + H^*$	1	0	0	0	0	(r10)
$SiH_2^* + {}^* \rightarrow SiH^* + H^*$	1	1	1	2	2	(r11)
$SiH^* \rightarrow Si(s) + H^*$	1	1	1	2	2	(r12)
+ - - - - - - - - - - - - - - - - - -	$\sigma_{\alpha\alpha}$	$\sigma_{\beta\beta}$	$\sigma_{\gamma\gamma}$	$\sigma_{\delta\delta}$	$\sigma_{\epsilon\epsilon}$	
$SiH_4 + 4^* \rightarrow Si(s) + 4H^*$	1	0	0	0	0	(α)
$SiH_2 + 2^* \rightarrow Si(s) + 2H^*$	0	1	0	0	0	(β)
$Si_2H_6 + 2^* \rightarrow Si(s) + 2H^* + SiH_4$	0	0	1	0	0	(γ)
$H_3SiSiH + 4^* \rightarrow 2Si(s) + 4H^*$	0	0	0	1	0	(δ)
$H_2SiSiH_2 + 4^* \rightarrow 2Si(s) + 4H^*$	0	0	0	0	1	(ϵ)
$H^* \rightleftarrows H^e + {}^*$	2	1	1	2	2	(r13)
$H^* + H^e \rightleftarrows H_2 + {}^*$	2	1	1	2	2	(r14)
+ - - - - - - - - - - - - - - - - - -						
$SiH_4 \rightarrow Si(s) + 2H_2$						(αα)
$SiH_2 \rightarrow Si(s) + H_2$						(ββ)
$Si_2H_6 \rightarrow Si(s) + H_2 + SiH_4$						(γγ)
$H_3SiSiH \rightarrow 2Si(s) + 2H_2$						(δδ)
$H_2SiSiH_2 \rightarrow 2Si(s) + 2H_2$						(ϵϵ)

The global reactions (α–ϵ), built up from elementary steps and symbolized by the columns with stoichiometric numbers σ_α to σ_ϵ, describe the decomposition of silane, silylene, disilane, silylsilylene, and disilene into solid silicon and hydrogen adatoms. The decomposition reactions of surface trihydride, SiH_3^*, dihydride, SiH_2^*, and monohydride, SiH*, species are considered to be potentially fast compared to the adsorption reactions of the former gas-phase species. The rates of the global reactions (α–ϵ) are consequently given by the rates of the corresponding adsorption reactions (r5–r9), as follows from the stoichiometric numbers. Together with the elementary reactions (r13) and (r14), these global reactions take part in the global deposition paths (αα–ϵϵ), symbolized by the columns with stoichiometric numbers $\sigma_{\alpha\alpha}$ to $\sigma_{\epsilon\epsilon}$. In these sequences, the global reactions (α–ϵ) are now potentially fast compared to the desorption of hydrogen, or more specifically, the excitation of a covalently bound hydrogen adatom given by reaction (r13). Note that the latter is not a rate-determining step in the classical sense of the term, since the steps leading to hydrogen adatom formation are not equilibrated.[62]

In the present work silane adsorption is considered to proceed through reaction (r5) of Table III, which is in line with the work of Holleman and Verweij.[5] In this reaction silane is assumed to adsorb dissociatively, forming a surface trihydride species, and a hydrogen adatom. The inclusion of the adsorption reaction given by Eq. 1

$$SiH_4 + {}^* \rightarrow SiH_2^* + H_2 \qquad [1]$$

as proposed by Farnaam and Olander[18] and by Gates et al.[12,13] did not further improve the modeling results. An

indication for the irreversibility of the adsorption of silane was provided by TAP (Temporal Analysis of Products) alternating pulse experiments with silane and deuterium, revealing no desorption of deuterated silicon containing gas-phase species.[7,63]

For disilane adsorption several mechanisms can be found in the literature. Using H_2 TPD, Gates[9] proposed an adsorption reaction involving the formation of two surface trihydride species

$$Si_2H_6 + 2* \rightarrow 2SiH_3^* \quad [2]$$

Vibrational spectroscopy provided additional evidence for the occurrence of this reaction on Si(111)-(7 × 7).[64,65]

Kulkarni et al.[66,67] identified three distinct temperature regions for disilane adsorption on Si(111)-(7 × 7) using modulated molecular beam spectroscopy (MMBS). At temperatures below 675 K, a fully hydrogenated inert surface resulted from disilane adsorption, and silicon deposition could be neglected. Between 675 and 775 K slight silane evolution was observed. This was attributed to the decomposition of disilane emitting a silane molecule and chemisorbing a dihydride species, see reaction (r7) in Table III, followed by fast dissociation of the surface dihydride species. The apparent activation energy amounted to ~13 kJ mol^{-1}. At temperatures above 775 K, disilane adsorption was believed to occur via two competing mechanisms, both producing silane. One mechanism again involved the decomposition into silane and chemisorbed dihydride, which was predicted to be the main channel of silicon growth from disilane at temperatures between 773 and 1173 K. The chemisorbed dihydride then rapidly reacts to two hydrogen adatoms, which in turn serve as active sites for the second chemisorption mechanism

$$Si_2H_6 + 2H* \rightarrow 2SiH_4 + 2* \quad [3]$$

This process appeared to be more active at H removal from the surface than the usual way of associative hydrogen desorption.

In the present work disilane adsorption is considered to proceed through reaction (r7) of Table III. This reaction is treated as an elementary reaction but will undoubtedly comprise a number of elementary reactions in reality, as evidenced by the MMBS experiments of Kulkarni et al.[66,67] and the small, negative apparent activation energies generally observed.[9,64,65]

The adsorption of silylene, silylsilylene, and disilene is taken into account through reactions (r6), (r8), and (r9) of Table III, all of them producing one or more surface dihydride species. It is assumed that the adsorption of these reactive gas-phase intermediates takes place without simultaneous evolution of a silicon-containing gas-phase species or direct release of molecular hydrogen. Silylsilylene and disilene are considered to adsorb via dual-site mechanisms. Since the subsequent surface decomposition reactions are considered potentially fast, the type of surface species formed during each of these adsorption reactions becomes completely irrelevant.

Trihydride decomposition is assumed to occur through interaction with a vacant surface site without direct release of molecular hydrogen into the gas phase, reaction (r10) of Table III, which is completely in line with the results of Greenlief et al.[10] and Gates et al.[11]

Dihydride decomposition is known to proceed via at least two mechanisms. Gates et al.[11] postulated that a surface dihydride species decomposes via interaction with a vacant surface site [reaction (r11) of Table III]. An additional reaction observed for dihydride decomposition involves direct release of molecular hydrogen into the gas phase[10,11,68]

$$2SiH_2^* \rightarrow 2SiH* + H_2 \quad [4]$$

As indicated before, silicon growth is controlled predominantly by the rate of hydrogen desorption in the complete range of process conditions investigated, whereas the surface concentrations of the silicon hydride species are negligible. Due to the abundance of vacant surface sites compared to sites occupied by dihydride species, reaction (r11) of Table III is more likely to occur than the reaction given in Eq. 4. However, the use of the second-order dihydride decomposition reaction does not lead to essentially different model equations than those used here, indicating the insensitivity of the overall deposition kinetics for the kinetics of dihydride decomposition.

In the present work monohydride species, SiH*, and hydrogen adatoms, H*, are treated as separate surface species, although they are experimentally indistinguishable. The basic difference between these species is that the hydrogen atom in SiH* is bonded to a silicon adatom, whereas H* denotes a hydrogen atom bonded to a silicon surface atom. Monohydride decomposition is considered to proceed via reaction (r12) of Table III.

Kinetic Parameter Determination in the Absence of Gas-Phase Reactions

Model equations.—In the absence of gas-phase reactions, silicon deposition is completely accounted for by heterogeneous decomposition of silane. Silane, hydrogen, and argon form the only significant gas-phase components. Since silicon deposition from silane is not significantly accompanied with gas/solid mass-transfer resistances, the gas-phase composition governing the deposition rate in the center of the reactor is identical to that at the outlet of the reactor, being calculated from the outlet molar flow rates of silane and argon and the outlet molar flow rate of hydrogen obtained from a hydrogen mass balance over the reactor.

The mechanism of silicon deposition from silane is represented by the columns with stoichiometric numbers σ_α and $\sigma_{\alpha\alpha}$ in Table III. As noted earlier, hydrogen adatoms form the only kinetically significant surface species at the experimental conditions applied. Starting from this mechanism with global reaction (α) and elementary reactions (r13) and (r14) as kinetically significant reactions, the following steady-state mass balance for hydrogen adatoms can be written, provided the Langmuir assumptions hold

$$4k_5C_{SiH_4}\frac{L_*^2}{L_t} - k_{13}L_{H^*} + k_{-13}L_{H^e}L_* - k_{14}L_{H^*}L_{H^e} + k_{-14}C_{H_2}L_* = 0 \quad [5]$$

Here L_i is the surface concentration of component i and L_t the total surface concentration of active sites available for adsorption or reaction. The first term on the left side represents the rate of hydrogen adatom production via global reaction (α), which is equal to four times the rate of silane adsorption via reaction (r5). Each silane molecule converted to solid silicon produces four hydrogen adatoms [see global reaction (α)]. Silane adsorption is considered to proceed on nearest neighbor vacant surface sites or on so-called dual adsorption sites. The rate of adsorption is therefore proportional to the concentration of dual adsorption sites and hence to L_t instead of L_t^2, as it might appear *prima facie*. This is in line with the results of the treatment of a dual-site adsorption mechanism by Boudart and Djéga-Mariadassou.[69] The four terms remaining on the left side of Eq. 5 represent the hydrogen adatom formation and disappearance rates corresponding to the elementary steps of reactions (r13) and (r14) and are written in a straightforward way following the law of mass action, i.e., assuming that the mean-field approximation holds.

It has been pointed out that desorption of molecular hydrogen via reaction of a delocalized hydrogen atom with a localized hydrogen adatom, reaction (r14), is potentially very fast compared to formation of a delocalized hydrogen atom, reaction (r13) of Table III. An expression for the concentration of delocalized hydrogen atoms consequently is obtained by applying the steady-state approximation for this species

$$L_{H^e} = \frac{k_{13}L_{H^*} + k_{-14}C_{H_2}L_*}{k_{-13}L_* + k_{14}L_{H^*}} \quad [6]$$

Substituting this expression into Eq. 5 and assuming that the recombination of a localized hydrogen adatom with a delocalized hydrogen atom is potentially very fast compared to the interaction of a delocalized hydrogen atom with a vacant surface site,[14,15] i.e.

$$k_{-13}L_* << k_{14}L_{H*} \quad [7]$$

finally results in the following mass balance for hydrogen adatoms

$$4k_5C_{SiH_4}\frac{L_*^2}{L_t} - 2k_{13}L_{H^*} + \frac{2k_{13}K_HC_{H_2}L_*^2}{L_{H^*}} = 0 \quad [8]$$

In this expression, K_H is the equilibrium coefficient of molecular hydrogen adsorption, defined as

$$K_H = \frac{k_{-13}k_{-14}}{k_{13}k_{14}} \quad [9]$$

An additional expression relating the concentration of hydrogen adatoms with that of vacant surface sites is obtained by equating the summed concentrations with the total concentration of active surface sites

$$L_t = L_* + L_{H*} \quad [10]$$

The concentration of excited hydrogen atoms, L_{H^e}, has been omitted from this equation because of its small value as compared to L_{H*} and L_*. Moreover, these species are not bonded to the surface in the usual localized way. In the present work, L_t is taken to be equal to 1.13×10^{-5} mol m^{-2}, corresponding to the number density of dangling bonds on Si(100), 6.8×10^{18} m^{-2}.[70] The reaction model makes no assumptions about the details of the surface structure.

The surface concentrations of hydrogen adatoms and vacant surface sites are now obtained by solving Eq. 8 and 10. Assuming that each silane molecule reacting at the surface leads to incorporation of a silicon atom into the growing layer, the silicon growth rate in units m s^{-1}, R_{Si}, which is experimentally determined from the growth rate in units kg s^{-1}, Gr_{Si}, can be calculated according to

$$R_{Si} = \frac{Gr_{Si}}{\rho_{Si}A_{sam}} = k_5C_{SiH_4}\frac{L_*^2}{L_t}\frac{M_{Si}}{\rho_{Si}} \quad [11]$$

Regression analysis.—The model equations given by Eq. 8, 10, and 11 feature details of silane adsorption and hydrogen adsorption/desorption only. The rate coefficient of the dual-site dissociative adsorption of silane, k_5 (m^3 mol^{-1} s^{-1}), and of the excitation of a hydrogen adatom into a delocalized state, k_{13} (s^{-1}), were expressed according to transition state theory in terms of a standard activation entropy, $\Delta^\ddagger S^0$, and a standard activation enthalpy, $\Delta^\ddagger H^0$.[71] The equilibrium coefficient corresponding to the dissociative adsorption of hydrogen, K_H (m^3 mol^{-1}), was expressed in Van't Hoff form in terms of a standard adsorption entropy, Δ_aS^0, and a standard adsorption enthalpy, Δ_aH_0.

In the literature it is generally agreed that silane adsorption is not or is only slightly activated. Reported activation energies range between 0 and 17 kJ mol^{-1}.[32,72,73] Hence, the standard activation enthalpy of silane adsorption, $\Delta^\ddagger H_5^0$, was kept fixed at zero during the regression.

The obtained kinetic and thermodynamic parameter estimates with their corresponding 95% confidence intervals are shown in the second column of Table IV. The F value of the regression was 3200. The largest value for the binary correlation coefficient between two parameter estimates occurred for the standard activation entropy of silane adsorption and the reparameterized standard entropy change of hydrogen adsorption and amounted to 0.90.

Kinetic Parameter Determination in the Presence of Gas-Phase Reactions

Model equations.—Due to the high surface reaction probability of the gas-phase intermediates formed during the pyrolysis of silane, it is necessary to account for the mass-transfer resistances of these species during the simulation of the kinetic experiments performed in the laboratory reactor. The shape of the concentration profiles was shown to be a complex function of the Damköhler-II number based on the surface kinetics and a modified Thiele modulus based on the gas-phase kinetics.[6,7] Weerts et al.[6] developed a one-dimensional model for the laboratory reactor taking into account these so-called irreducible mass-transport limitations in an appropriate way and providing both the silicon growth rate on the wafer and the outlet flow rates of the gas-phase components. The former is calculated according to the right side of Eq. 11 with extra terms accounting for silicon deposition from silylene, disilane, silylsilylene, and disilene. The mass transfer between gas-phase and deposition surface is accounted for by considering molecular diffusion with simultaneous gas-phase reactions. The inlet and outlet molar flow rates of each gas-phase component are treated as source terms in the corresponding continuity equations. Multicomponent diffusion effects are accounted for by the Stefan–Maxwell equations. For both the wafer and the reactor wall surfaces the continuity equations for the surface components follow from the straightforward application of the pseudo-steady-state approximation for these species.

Table IV. Kinetic and thermodynamic parameter estimates with approximate individual 95% confidence intervals obtained in the absence and in the presence of gas-phase reactions.[a]

Parameter	Region without gas-phase reactons[c]	Region including gas-phase reactions[d]
$\Delta^\ddagger S_5^0$ (J mol^{-1} K^{-1})	-172 ± 3	-172[b]
$\Delta^\ddagger H_5^0$ (kJ mol^{-1})	0[b]	0[b]
$\Delta^\ddagger S_{13}^0$ (J mol^{-1} K^{-1})	-33 ± 16	-40 ± 11
$\Delta^\ddagger H_{13}^0$ (kJ mol^{-1})	186 ± 14	180 ± 10
$\Delta_aS_H^0$ (J mol^{-1} K^{-1})	-336 ± 55	-327 ± 25
$\Delta_aH_H^0$ (kJ mol^{-1})	-369 ± 50	-361 ± 23

[a] Standard state 1 mol m^{-3}, $\theta = 0.5$.
[b] Fixed.
[c] 150 experiments conducted in the range of experimental conditions listed in the second column of Table I.
[d] 210 experiments conducted in the complementary ranges of experimental conditions listed in the second and third column of Table I.

The kinetic model used consists of the elementary gas-phase reactions of Table II coupled to the global adsorption reactions (α–ϵ) and the elementary reactions (r13) and (r14) of the surface reaction network given in Table III. In total, six gas-phase species are involved, i.e., SiH_4, SiH_2, Si_2H_6, H_3SiSiH, H_2SiSiH_2, and H_2, and besides vacant surface sites, only one kinetically significant surface species exists, i.e., hydrogen adatoms.

The homogeneous net production rates of these gas-phase species are derived following the law of mass action for the rates of the elementary gas-phase steps in Table II. Since the rates of the global reactions (α–ϵ) are determined by the rates of the corresponding elementary adsorption reactions, reactions (r5–r9), the heterogeneous net production rates of the gas-phase species are derived following the law of mass action for the rates of the corresponding adsorption reactions. The heterogeneous net production rate of molecular hydrogen is calculated from those of the silicon-containing species using the stoichiometry of the global deposition paths ($\alpha\alpha$–$\epsilon\epsilon$) of Table III. An expression for the net production rate of hydrogen adatoms can be derived in a similar way as outlined previously, but now with additional terms for the rates of hydrogen adatom production via the global adsorption reactions of silylene, disilane, silylsilylene, and disilene (β–ϵ).

Since the irreducible mass-transport limitations are accounted for during the analysis of the laboratory reactor data in case gas-phase reactions are important, intrinsic values for the kinetic parameters are obtained. These kinetic parameters can therefore be applied in a straightforward

way for the design and analysis of an industrial hotwall multiwafer LPCVD reactor.[19,20]

Regression analysis.—Since the total number of rate and equilibrium coefficients featured in the model equations is 15, a set of 30 kinetic and thermodynamic parameters would have to be estimated. This number could be reduced, however, by the use of thermodynamic and physicochemical relations and a formal sensitivity analysis.

The rate coefficients of the unimolecular gas-phase steps, k_1, k_{-2}, k_3, and k_4 (s^{-1}), were calculated using an empirical relation accounting for the pressure falloff behavior of these steps[7,8]

$$k_k = A_k\left(\sum_{i=1}^{NG}\lambda_i p_i\right)^{B_{1,k}} \exp\left\{-\frac{E_{a,k} + B_{2,k}\ln\left(\sum_{i=1}^{NG}\lambda_i p_i\right) + B_{3,k}\left(\ln\left(\sum_{i=1}^{NG}\lambda_i p_i\right)\right)^2}{RT}\right\} \quad [12]$$

For each of the unimolecular gas-phase steps the values of the pressure correction constants $B_{1,k}$ to $B_{3,k}$ are listed in Table II. The values of the corresponding Arrhenius parameters are listed in Table V, with the exception of the pre-exponential factor for the silane dissociation, reaction (r1) in Table II, which amounted to 3.53×10^8 s^{-1}. These values were obtained by regression of falloff data calculated on the basis of the RRKM theory in the pressure range 1–1000 Pa and in the temperature range 800–1000 K using transition state parameters given in the literature.[74-76] The collisional deactivation efficiencies, λ_i, were set to 1.0, except those for the small molecules hydrogen and argon which were put equal to 0.3.

Through a sensitivity analysis small sensitivities for all gas-phase reaction rate coefficients were detected except for that corresponding to the initiation step, reaction (r1) in Table II. For this reason the pre-exponential factors A_{-2}, A_3, and A_4, as well as the activation energies $E_{a,-2}$, $E_{a,3}$, and $E_{a,4}$ were kept fixed at the RRKM based values listed in Table V, whereas the pre-exponential factor of the initial step in silane pyrolysis, A_1, was adjusted during the regression of the laboratory data. Due to a strong correlation between the activation energy of the initial step in silane pyrolysis, $E_{a,1}$, and the standard enthalpy change of hydrogen adsorption, $\Delta_a H^0_H$, the former was not adjusted either but kept fixed at the RRKM value listed in Table V.

The rate coefficients of the reverse gas-phase steps, k_{-1}, k_2, k_{-3} (m^3 mol^{-1} s^{-1}), and k_{-4} (s^{-1}), were calculated from the equilibrium constants and the forward step rate coefficients, with the former calculated at the reaction temperature using the most recent thermodynamic data base of Coltrin et al.[49,51]

The rate coefficients of the adsorption of the gaseous silicon hydrides, k_5 to k_9, were expressed in Arrhenius form. The corresponding activation energies, $E_{a,5}$ to $E_{a,9}$, were kept fixed at zero during the regression. The pre-exponential factor A_5 was calculated from the estimated standard activation entropy derived in the region where gas-phase reactions can be omitted. The pre-exponential factors A_6 to A_9 were kept fixed at the values calculated from kinetic gas theory for $T = 900$ K and an initial sticking probability equal to 0.1 in case of disilane and 1.0 in case of silylene, silylsilylene, and disilene.

By sensitivity analysis, large sensitivities for both the rate coefficient k_{13}, corresponding to the excitation of a hydrogen adatom, and the equilibrium coefficient K_H, reflecting molecular hydrogen adsorption, were detected. Therefore, expressing both coefficients in Arrhenius form, the pre-exponential factors A_{13} and A_H with the corresponding $E_{a,13}$ and $\Delta_a H^0_H$ were adjusted during the regression of the kinetic experiments. The number of kinetic and thermodynamic parameters to be estimated could thus be reduced to five, i.e., A_1, A_{13}, A_H, $E_{a,13}$, and $\Delta_a H^0_H$.

The final kinetic and thermodynamic parameter estimates with their corresponding 95% confidence intervals are shown in Table V. The F value of the regression amounted to 59,000. The largest value for the binary correlation coefficient between two parameter estimates occurred for the reparameterized pre-exponential factors corresponding to hydrogen adsorption and to the excitation of a hydrogen adatom into a delocalized state and amounted to 0.83. Parity diagrams of the calculated vs. the observed silicon growth rates and Si_2H_x outlet molar flow rates can be found in Weerts et al.[6] The absence of systematic deviations reflects the adequacy of the model. This is also illustrated in Fig. 1, 3, 4, and 5.

Table V. Final kinetic and thermodynamic parameter estimates with their approximate individual 95% confidence intervals obtained from a regression analysis of 210 experiments in the complementary ranges of experimental conditions listed in the second and third column of Table I.[a]

Reaction, equilibrium	A or A^b estimate with 95% confidence interval (s^{-1}, m^3 mol^{-1}, or m^3 mol^{-1} s^{-1})	E_a or $\Delta_a H^0$ estimate with 95% confidence interval (kJ mol^{-1})
(r1)	(1.28 ± 0.03) 10^{10}	215.8
(r-2)	3.53 10^9	163.3
(r3)	9.68 10^9	180.6
(r4)	6.02 10^4	4.2
(r5)	3.89 10^4	0.0
(r6)	1.76 10^7	0.0
(r7)	1.23 10^6	0.0
(r8)	1.25 10^7	0.0
(r9)	1.25 10^7	0.0
(r13)	7.8 ± 0.4 [b]	188 ± 10
(H)	(3.5 ± 0.5) 10^3 [b]	-361 ± 23

[a] Gas-phase and surface reaction networks shown in Tables II and III.

[b] The non-reparameterized pre-exponential factors can be deduced from the reparameterized ones according to $A_{13} = A_{13}/\exp(E_{a,13}/RT_m)$ and $A_H = A_H/\exp(\Delta_a H^0_H/RT_m)$ with $T_m = 914.8$ K, the average temperature of the experiments.

Simulation Results

The silane conversion, the Si_2H_x selectivity, and the silicon growth rate calculated using the complete kinetic network shown in Tables II and III and the reactor model accounting for the irreducible mass-transport limitations are drawn as full lines in Fig. 1, 3, 4, and 5.

Figure 5 demonstrates that the kinetic model adequately describes the dependence of silane conversion on silane space time over a broad range of temperatures at 50 Pa, even at silane conversions as high as 64%. The simulations confirm the existence of a differential operating regime with respect to silane conversion at the lower temperatures considered. Figure 1 shows the silicon growth rate as a function of silane conversion at 50 Pa. Obviously, at each of the considered temperatures the agreement between experimental and calculated growth rate is good. This implicitly means that the dependence between silicon growth rate and silane space time is simulated correctly as well over this range of temperatures.

Figure 4 shows the effect of inlet hydrogen-to-silane ratio on the silicon growth rate at 912 K and total pressures of 25 and 50 Pa. In this regime gas-phase reactions are not important and silicon deposition is predominantly determined by the heterogeneous decomposition of silane. Hence, the rate of silicon deposition equals the rate of silane adsorption [see reaction (r5) in Table III], and depends on the concentration of vacant surface sites squared. Due to the enhanced adsorption of molecular hydrogen with increasing inlet hydrogen-to-silane ratio, the fraction of vacant surface sites decreases, thereby slowing down the adsorption of silane and, hence, the deposition of silicon. The adequate simulation of the observed hydrogen inhibiting effect on the sili-

con growth rate shows that reaction (r5) and the reverse of reaction (r14) in Table III provide a good way to account for the competitive adsorption of silane and hydrogen.

Also, the effect of total pressure is adequately described. Even at pressures as high as 100 Pa the kinetic model provides a good description of the experimental data as shown in Fig. 3, where the silicon growth rate, the silane conversion, and the Si_2H_x selectivity are plotted vs. the silane space time at 963 K. Clearly, silicon growth rates as high as 1.5×10^{-9} m s^{-1} are simulated correctly by the model.

Assessment of Parameter Estimates

Examination of the individual kinetic and thermodynamic parameter estimates can further validate the reaction model shown in Tables II and III.

The estimated value of the pre-exponential factor of the initial reaction in silane pyrolysis, A_1 in Table V, deviates by almost a factor of forty from the value obtained from the RRKM analysis, giving rise to a similar discrepancy in the corresponding unimolecular rate coefficient, k_1. Applying Eq. 12 with the pressure correction constants and the RRKM-based Arrhenius parameters results in a k_1 value of 1.0×10^{-2} s^{-1} at an effective total pressure of 100 Pa and 900 K. In contrast, the estimated pre-exponential factor given in Table V gives rise to a k_1 value of 3.8×10^{-1} s^{-1}. An explanation for this discrepancy is that the former value is derived by means of RRKM analysis of experiments at much higher pressure and/or lower temperature than generally applied in LPCVD of polycrystalline silicon. The estimated value is in good agreement, however, with the value of 3.5×10^{-1} s^{-1} obtained by Holleman and Verweij[5] through fitting of the growth rate data in a conventional LPCVD reactor at 100 Pa total pressure and 898 K. Moreover, the same authors calculated values of 5.2 and 2.9×10^{-1} s^{-1} using Jasinski and Chu's[77] and Inoue and Suzuki's[42] values for the rate coefficient of the reverse step, k_{-1}, combined with the thermodynamic data of Kleijn.[21] Yeckel et al.[78] fitted the rate coefficient for silane decomposition to growth rate data obtained by Meyerson and Olbricht[79] for in situ doped polycrystalline silicon in an LPCVD reactor at 896 K, 13.3 Pa, and 100% silane. In case disilane was considered to contribute to the silicon deposition rate as well, a value of 3.9×10^{1} m^3 mol^{-1} s^{-1} was obtained, which can be transformed into a value of 5.2×10^{-1} s^{-1} for 100 Pa total pressure and 100% silane at the same temperature.

The small 95% confidence interval of the estimated standard activation entropy of silane adsorption, $\Delta^{\ddagger}S_5^0$ in the second column of Table IV, arises from keeping the value of the standard activation enthalpy of silane adsorption fixed during the regression. An upper limit for the standard activation entropy loss can be calculated by assuming that the transition state possesses neither translational nor external rotational degrees of freedom. On the basis of statistical thermodynamics, a value of 239 J mol^{-1} K^{-1} can be calculated for the summed contributions of translational and external rotational entropy of silane in the gas phase at 1 atm and 900 K. Transformation of the estimated value of Table IV from standard states of 1 mol m^{-3} to standard states of 1 atm, yields a value of -150 J mol^{-1} K^{-1}. The entropy loss indeed is smaller than 239 J mol^{-1} K^{-1}.

Another way to assess the physical meaning of the estimated standard activation entropy involves calculation of the initial sticking probability, s_0. The sticking probability at a given value of surface coverage, s, is defined as the net rate of adsorption divided by the rate of collision with the surface.[69] Using the relation between the initial sticking probability and the sticking probability at a given surface coverage for dissociative adsorption involving pairs of adjacent vacant surface sites[80] finally leads to the following expression for the initial sticking probability

$$s_0 = \frac{k_5 L_t}{\frac{1}{4}\sqrt{\frac{8RT}{\pi M_{Si_2H_4}}}} \qquad [13]$$

Substituting the appropriate equation for k_5 together with the estimates of Table IV into Eq. 13 yields an initial sticking probability equal to 2.3×10^{-3} at 900 K. It is important to realize that the same value applies to the reaction probability at zero coverage, γ^0. The reaction probability at a given value of surface coverage is defined as the ratio of the net rate of silicon growth divided by the rate of collision with the surface.[32,73] Because desorption of surface dihydride and monohydride species does not occur, the net rate of silicon growth is equal to the net rate of adsorption, see Eq. 11, and the values of reaction and sticking probability consequently coincide. Literature values for initial sticking and reaction probabilities range between 1×10^{-5} and 1×10^{-3}.[5,12,13,32,81] The calculated value of 2.3×10^{-3} is in good agreement with the values found by Buss et al.,[32] 1×10^{-3}, and Holleman and Verweij,[5] 8×10^{-4}.

The estimates of the Arrhenius parameters associated with the excitation of a hydrogen adatom into a delocalized state, A_{13} and $E_{a,13}$ in Table V, are in good agreement with the results of Sinniah et al.,[15] who experimentally obtained a pre-exponential factor equal to 2.2×10^{11} s^{-1} and an apparent activation energy of 188 kJ mol^{-1} for hydrogen desorption from Si(100).

Table IV lists the estimates obtained for k_{13} and K_H after regression of the data in the complete region, i.e., the region including gas-phase reactions and obtained from the estimates reported in Table V, as well as those estimated in the region where gas-phase reactions can be neglected. Clearly, the deviations between both sets of parameter estimates is very small. Within their 95% confidence intervals the parameter estimates of the two regions coincide.

The estimated standard reaction enthalpy of dissociative hydrogen adsorption, shown in the third column of Table IV, is in good agreement with the standard enthalpy change estimated according to D^0(H-H)-$2D^0$(Si-H), i.e., -314 kJ mol^{-1}. Keep in mind that the latter value represents an upper limit as it is based on an upper limit for the Si–H bond strength equal to 376 kJ mol^{-1}.[82]

Vannice et al.[83] showed that values obtained for $\Delta_a S^0$ must conform to certain rules and guidelines in order to have any physical meaning and thereby support the proposed reaction model. These rules and guidelines, originally postulated by Boudart et al.,[84] can be summarized as follows

$$0 < -\Delta_a S^0 < S_g^0 \qquad [14]$$

$$42 < -\Delta_a S^0 \leq 51 - 0.0014\,\Delta_a H^0 \qquad [15]$$

where S_g^0 is the entropy in the gas phase taken at 1 atm. The lower limit of Eq. 14 follows directly from the necessary loss of entropy when a molecule is transferred without dissociation from a three-dimensional to a two-dimensional phase. The upper limit expresses the fact that a molecule cannot lose more entropy than it possesses. The lower limit of Eq. 15 follows by calculating the entropy change which occurs when a gas condenses to a liquid at the critical state. The equality sign in this equation corresponds to physical adsorption of a wide variety of compounds on charcoal in less than a monolayer at 298 K.[85] Transformation of the estimated standard reaction entropy of dissociative hydrogen adsorption, $\Delta_a S_H^0$ in the third column of Table IV, from standard states of 1 mol m^{-3} to standard states of 1 atm, yields a value of -305 J mol^{-1} K^{-1}. This value fulfills the strict rule reflected by the lower limit of Eq. 14 as well as the less stringent guidelines represented by Eq. 15. However, the strict rule reflected by the upper limit of Eq. 14 is not satisfied. Using statistical thermodynamics, a value of 163 J mol^{-1} K^{-1} is calculated for the entropy of molecular hydrogen in the gas phase at 1 atm and 900 K, which is significantly below 305 J mol^{-1} K^{-1}.

Deposition Path Analysis and Relative Importance of Gas-Phase Reactions

Effect of space time.—Figure 3 shows the silicon growth rate, the silane conversion, and the Si_2H_x selectivity vs. the silane space time at 100 Pa and 963 K. The Si_2H_x selectiv-

ity here is defined as the ratio of net number of moles of silicon atoms in Si_2H_x (= Si_2H_6 + H_3SiSiH + H_2SiSiH_2) formed to the total number of moles of silicon atoms in SiH_4 converted. Under the conditions discussed in this paper it is a measure of the relative importance of gas-phase formation of Si_2H_x vs. disappearance via heterogeneous reactions of the silicon-containing species. As such it gives an indication of the contribution of Si_2H_x species to the overall deposition rate. The simulations have been extrapolated to zero space time. The silicon growth rate first increases from 12.7×10^{-10} m s^{-1} at zero space time to 17.1×10^{-10} m s^{-1} at 2.3 m^3 s mol^{-1} and then gradually decreases with increasing space time. The Si_2H_x selectivity starts at zero because SiH_2 needs to be formed first, almost instantaneously reaches a maximum value of 36%, and then strongly decreases with increasing space time.

At space times close to zero the silicon growth rate is determined by heterogeneous decomposition of silane and silylene only. The contribution from silylene to the silicon growth rate amounts to roughly 16%. With increasing space time the growth rate due to the gas-phase intermediates starts to increase as a result of the formation of disilane and disilene. The fraction of vacant surface sites is determined by the balance between consumption through adsorption of the various silicon-containing gas-phase species, reactions (r5–r9), and production through desorption of molecular hydrogen or more specifically through excitation of hydrogen adatoms, reaction (r13). With increasing space time the concentrations and, hence, the adsorption rates of disilane and disilene increase. The rate of hydrogen adatom excitation, however, is not directly effected by a change in space time, and the fraction of vacant surface sites consequently decreases, from 0.207 to 0.186. This decrease effects the growth rate contribution from silane, which decreases by approximately 24% in this stage of the deposition process. At the space time where the total growth rate due to the gas-phase intermediates has reached its maximum value, 2.8 m^3 s mol^{-1}, the contribution from silane to the total growth rate amounts to 55.8%, the remaining growth being built up of the contributions from silylene, 16.4%, disilane, 22.7%, and disilene, 5.0%. The contribution from silylsilylene is negligible. The growth rate contribution from the gas-phase intermediates thus is almost completely determined by the contributions from silylene and disilane. Upon further increasing the space time, the growth rate due to the gas-phase intermediates starts to decrease as a result of a decrease in the concentration of disilane in particular. The main cause for the decrease in the concentration of this species is twofold. The most obvious reason is the decreasing silane concentration with increasing space time. A second, less obvious reason is the increasing hydrogen concentration with increasing silane conversion. This reduces the overall collision efficiency of the reaction mixture and hence the unimolecular reaction rate coefficients, thereby slowing the gas-phase reactions. Concurrently with the decrease in the concentrations of silane, disilane, and also disilene, an increase in the fraction of vacant surface sites takes place as a result of a decrease in the adsorption rates of these species without a direct change in the rate of hydrogen adatom excitation.

A contribution analysis performed at the space time where the growth rate due to the gas-phase intermediates is maximal revealed that silane consumption occurs for 31% through homogeneous dissociation, see reaction (r1), for 28% through insertion of silylene, see reaction (r2), and for 41% via heterogeneous decomposition according to global reaction (α). Table VI summarizes the results of the contribution analysis. Instead of contribution percentages of the individual reaction steps, the contribution percentages obtained after summation over all gas-phase steps and over all surface steps are given in the table. Production contribution percentages for the gas-phase intermediates are omitted, because formation of these species is a matter of gas-phase kinetics only.

Production of silane occurs for 34% via homogeneous decomposition of disilane, see reaction (r-2), and for 66% via heterogeneous decomposition of disilane according to global reaction (γ). Formation of silylene is determined for 80% by homogeneous decomposition of silane and for 20% by homogeneous decomposition of disilane according to reaction (r-2). Silylene consumption takes place for 73% via insertion into silane, reaction (r2), and for 27% via heterogeneous decomposition according to global reaction (β). Insertion of silylene into molecular hydrogen, reaction (r-1), has no important contribution to the total disappearance of silylene at the conditions considered. This is consistent with the rather high value of 6.37 obtained for the dimensionless affinity of reaction (r1), indicating that the reverse step is not important. Dilution with large amounts of hydrogen obviously does not force the equilibrium of the initial silane pyrolysis reaction to the left. Except through reduction of the unimolecular gas-phase rate coefficients as a consequence of a lower collision efficiency, hydrogen has no further quenching effect on the gas-phase chemistry. Disilane consumption is for 31% accounted for by homogeneous decomposition into silane and silylene, for 8% by homogeneous decomposition into silylsilylene and hydrogen, and for 61% by heterogeneous decomposition. Insertion of silylene into silane accounts for 100% to the disilane production. Disilane formation via insertion of silylsilylene into hydrogen has no significant contribution, which also follows from the rather high value of 4.55 obtained for the dimensionless affinity of reaction (r3). The paths to and from H_3SiSiH are not discussed, because its contribution to the silicon growth rate is too low. Disilene disappearance occurs for 96% through isomerization toward silylsilylene, see reaction (r-4), and for 4% through heterogeneous decomposition. Production of disilene is fully accounted for by isomerization of silylsilylene. The dimensionless affinity of this isomerization reaction, reaction (r4), amounts to 0.04, indicating that its forward and backward steps proceed at the same rate and hence are equilibrated.

Table VI. Contribution analysis with respect to the consumption of the most important gas-phase species at silane space times of 2.8 and 40.4 m^3 s mol^{-1}. [a]

$V/F_{SiH_4,0}$ (m^3 s mol^{-1})	2.8		40.4	
X_{SiH_4} (%)	5.5		46.3	
	Surface (%)	Gas-phase (%)	Surface (%)	Gas-phase (%)
SiH_4				
Consumption	41	59	67	33
Production	66	34	76	24
SiH_2				
Consumption	27	73	55	45
Si_2H_6				
Consumption	61	39	72	28
H_2SiSiH_2				
Consumption	4	96	8	92

[a] Conditions: $SiH_4/Ar|_0$ = 4.5, $SiH_4/H_2|_0$ = 1.0, P_t = 100 Pa, T = 963 K. Surface-to-volume ratio A_s/V_g = 128.3 m^{-1}.

Table VI also shows the results of a contribution analysis with respect to the consumption of the most important gas-phase species at a much higher space time. Comparison shows that the relative importance of the gas-phase reactions reduces with increasing silane conversion. Hence, an unambiguous determination of the effects of either pressure or temperature on the relative importance of gas-phase reactions needs to be performed at a similar silane conversion.

Effect of temperature.—The total contribution to the growth rate from gas-phase intermediates is independent of temperature. It can be shown that this independency of temperature can be attributed in first approximation to the roughly equal activation energies of the gas-phase decomposition of silane and the first-order desorption of hydrogen, viz. Table V. With varying temperature a change in the most contributing gas-phase intermediate takes place. At 888 K disilane contributes 78% and silylene 17%

to the growth rate due to gas-phase intermediates, whereas at 963 K these percentages amount to 42 and 51%, respectively. Since the adsorption reactions of silylene and disilane are kinetically equivalent in the sense that both are nonactivated and require the same number of vacant surface sites, this effect of temperature has to be explained by the ratio between the gas-phase concentrations of silylene and disilane. An expression for this ratio can be derived from a pseudo-steady-state mass balance for disilane

$$k_2 C_{SiH_4} C_{SiH_2} + k_{-3} C_{H_3SiSiH} C_{H_2} - k_{-2} C_{Si_2H_6} - k_3 C_{Si_2H_6} - k_7 C_{Si_2H_6} L_* \frac{A_d}{V_g} - C_{Si_2H_6} \frac{F_v}{V_g} = 0 \quad [16]$$

in which the last term on the left side denotes the molar flow rate of disilane at the reactor outlet in units mol m^{-3} s^{-1} and A_d/V_g represents the surface-to-volume ratio of the laboratory reactor. The contribution analysis discussed in the previous section showed that production of disilane is completely accounted for by silylene insertion into silane, reaction (r2). Disilane disappearance, on the other hand, takes place through homogeneous decomposition into silane and silylene, reaction (r-2), through heterogeneous decomposition according to global reaction (γ), and to a lesser extent via homogeneous decomposition into silylsilylene and hydrogen, see reaction (r3). The contribution of the outlet molar flow rate to the total disappearance of disilane is typically less than 2% and is therefore omitted in the mass balance given by Eq. 16. Rearrangement of the terms left at the left side results in the following expression for the ratio between the silylene and disilane concentration

$$\frac{C_{SiH_2}}{C_{Si_2H_6}} = \frac{k_{-2} + k_3 + k_7 L_* \frac{A_d}{V_g}}{k_2 C_{SiH_4}} \quad [17]$$

The denominator is almost independent of temperature, since both the second-order rate coefficient k_2 and the silane concentration C_{SiH_4} hardly change with temperature. On the other hand, all individual terms of the numerator increase with increasing temperature. The first-order rate coefficients k_{-2} and k_3 have activation energies of at least 163.3 and 180.6 kJ mol^{-1} (see Table V). The actual activation energies are even higher due to their dependence on effective pressure. The third term in the numerator increases due to the increase in the fraction of vacant surface sites with temperature. As mentioned earlier, the fraction of vacant surface sites is determined by the balance between consumption through adsorption of the various silicon-containing gas-phase species, reactions (r5–r9), and production through desorption of molecular hydrogen or more specifically through excitation of hydrogen adatoms, reaction (r13). As hydrogen adatom excitation is activated, $E_{a,13}$ = 188 kJ mol^{-1}, and adsorption of the silicon hydride species is nonactivated, higher temperatures lead to higher fractions of vacant surface sites. In this way it can be understood that with rising temperature the ratio of silylene concentration to disilane concentration increases and hence the relative contribution of silylene to the silicon growth rate.

Since SiH_4, H_3SiSiH, and H_2SiSiH_2 adsorb via dual-site adsorption mechanisms, the effect of increasing θ_* is more pronounced for these species than for SiH_2 and Si_2H_6, occupying only one vacant site upon adsorption. The effects associated with the higher concentrations of the gas-phase intermediates at the higher temperatures are not considered in the previous discussion. Naturally, these effects positively influence the adsorption rates and hence the growth rates from the intermediates, thereby slightly decreasing the fraction of vacant surface sites.

Effect of pressure.—The total contribution to the growth rate from gas-phase intermediates rises with total pressure. As for the situation of varying temperature, a change in the most contributing gas-phase intermediate occurs with varying total pressure. At 50 Pa silylene contributes 83% and disilane 16% to the growth rate due to gas-phase intermediates, whereas at 100 Pa these percentages amount to 51 and 42%, respectively. This effect can again be explained by the ratio between the gas-phase concentrations of silylene and disilane. This can be verified with the help of Eq. 17. C_{SiH_4} increases with increasing pressure. Also, the rate coefficients k_2, k_{-2}, and k_3 increase with increasing pressure because of their falloff behavior. However, higher pressures lead to a decrease in the fraction of vacant surface sites, since the gas-phase concentrations and hence the adsorption rates of all silicon hydride species increase with increasing pressure, whereas the rate of hydrogen adatom excitation is not directly effected. Therefore, the heterogeneous term $k_7 L_* A_d/V_g$ decreases with increasing pressure. Because the heterogeneous term is significantly larger than the sum of the homogeneous terms in the numerator, the decrease in the former exceeds the increase in the latter, thereby effectively lowering the numerator with pressure. Thus, with rising pressure the ratio of silylene concentration to disilane concentration decreases and hence the relative contribution of silylene to the silicon growth rate.

Conclusions

The intrinsic kinetics of the deposition of polycrystalline silicon can conveniently be studied in a continuous flow perfectly mixed reactor. In contrast to the conventional hotwall multiwafer LPCVD reactor generally used for kinetic investigations of this reaction, such a reactor provides local deposition rates combined with corresponding gas-phase compositions. The obtained data can readily be analyzed with a reactor model in which only binary diffusion coefficients figure as transport parameters. The latter can be calculated independently.

An adequate description of the polycrystalline silicon deposition process from silane over a broad range of conditions is possible with a minimum set of kinetically significant reactions in the gas-phase as well as at the surface. A four-step elementary gas-phase reaction network coupled to a ten-step elementary surface-reaction network provides such a description. The gas-phase reaction network considers dissociation of silane into silylene and hydrogen, formation of disilane from silane and silylene, subsequent decomposition of disilane into silylsilylene and hydrogen, and isomerization of silylsilylene into disilene. Pressure falloff effects on these reactions are accounted for using RRKM theory. The surface reaction network considers dual-site adsorption of silane, silylsilylene, and disilene, single-site adsorption of silylene and disilane, subsequent decomposition of the surface hydride species, and adsorption/desorption of molecular hydrogen. The latter is assumed to take place in two steps according to the band model of Sinniah et al.[14,15] As all decomposition reactions of surface hydride species are considered to be potentially much faster than the hydrogen desorption step, hydrogen adatoms are the only kinetically significant adsorbed species on the silicon surface. The involved kinetic and thermodynamic parameter estimates exhibit good statistical significance and are physically reasonable, except for the change in standard entropy for hydrogen adsorption.

In the range of silane conversions applied, the relative importance of gas-phase intermediates for silicon deposition decreases with increasing conversion and decreasing total pressure and is independent of temperature. Silylene and disilane are by far the most contributing gas-phase intermediates. The total contribution of these species to the silicon growth rate amounts to between 1 and 44%, depending on the operating conditions. Moreover, the ratio between the growth rates from silylene and disilane is affected by a change in either of the process variables considered, i.e., space time, total pressure, and temperature. It increases with increasing temperature and space time, or conversion, and with decreasing total pressure.

Manuscript submitted August 21, 1996; revised manuscript received November 4, 1997.

LIST OF SYMBOLS

A pre-exponential factor, reaction dependent
A_d total deposition surface area, m^2
A_{sam} geometric surface area of substrate, m^2
B_1 pressure correction constant for falloff
B_2 pressure correction constant for falloff, J mol^{-1}
B_3 pressure correction constant for falloff, J mol^{-1}
C_i gas-phase concentration of component i, mol m^{-3}
$C_{i,0}$ inlet gas-phase concentration of component i, mol m^{-3}
E_a Arrhenius activation energy, J mol^{-1}
F ratio of the mean regression sum of squares to the mean residual sum of squares
$F_{i,0}$ inlet molar flow rate of component i, mol s^{-1}
F_v volumetric flow rate, m^3 s^{-1}
Gr_{Si} silicon growth rate, kg s^{-1}
k reaction rate coefficient, reaction dependent
K_H equilibrium coefficient for molecular hydrogen adsorption, m^3 mol^{-1}
L_i surface concentration of component i, mol m^{-2}
L_t total surface concentration of active sites available for adsorption or reaction, mol m^{-2}
M_i molar mass of component i, kg mol^{-1}
NG number of gas-phase components
p_i partial pressure of component i, Pa
P_t total pressure, Pa
R gas constant, J mol^{-1} K^{-1}
R_{Si} silicon growth rate, m s^{-1}
s sticking probability
s_0 initial sticking probability
S_g^0 standard entropy in the gas-phase, J mol^{-1} K^{-1}
$S_{Si_2H_x}$ selectivity toward Si_2H_x
T temperature, K
T_m average temperature of experiments, K
V geometric reactor volume, m^3
V_g gas-phase reaction volume, m^3
X_{SiH_4} conversion of silane

Greek

γ^0 initial reaction probability
$\Delta_a H^0$ standard adsorption enthalpy, J mol^{-1}
$\Delta^{\ddagger} H^0$ standard activation enthalpy, J mol^{-1}
$\Delta_a S^0$ standard adsorption entropy, J mol^{-1} K^{-1}
$\Delta^{\ddagger} S^0$ standard activation entropy, J mol^{-1} K^{-1}
θ fractional surface coverage
λ_i collisional deactivation efficiency of component i
ρ_{Si} density of solid silicon, kg m^{-3}
σ stoichiometric number

REFERENCES

1. C. H. J. van den Brekel and L. J. M. Bollen, *J. Cryst. Growth*, **54**, 310 (1981).
2. W. A. P. Claassen, J. Bloem, W. G. J. N. Valkenburg, and C. H. J. van den Brekel, *J. Cryst. Growth*, **57**, 259 (1982).
3. K. F. Jensen and D. B. Graves, *J. Electrochem. Soc.*, **130**, 1950 (1983).
4. K. F. Roenigk and K. F. Jensen, *J. Electrochem. Soc.*, **132**, 448 (1985).
5. J. Holleman and J. F. Verweij, *J. Electrochem. Soc.*, **140**, 2089 (1993).
6. W. L. M. Weerts, M. H. J. M. de Croon, and G. B. Marin, *Chem. Eng. Sci.*, **51**, 2583 (1996).
7. W. L. M. Weerts, Ph.D. Thesis, Eindhoven University of Technology, Eindhoven, The Netherlands (1995).
8. P. J. Robinson and K. A. Holbrook, *Unimolecular Reactions*, Wiley, New York (1972).
9. S. M. Gates, *Surf. Sci.*, **195**, 307 (1988).
10. C. M. Greenlief, S. M. Gates, and P. A. Holbert, *J. Vac. Sci. Technol. A*, **7**, 1845 (1989).
11. S. M. Gates, C. M. Greenlief, and D. B. Beach, *J. Chem. Phys.*, **93**, 7493 (1990).
12. S. M. Gates, C. M. Greenlief, D. B. Beach, and P. A. Holbert, *J. Chem. Phys.*, **92**, 3144 (1990).
13. S. M. Gates, C. M. Greenlief, S. K. Kulkarni, and H. H. Sawin, *J. Vac. Sci. Technol. A*, **8**, 2965 (1990).
14. K. Sinniah, M. G. Sherman, L. B. Lewis, W. H. Weinberg, J. T. Yates, and K. C. Janda, *Phys. Rev. Lett.*, **62**, 567 (1989).
15. K. Sinniah, M. G. Sherman, L. B. Lewis, W. H. Weinberg, J. T. Yates, and K. C. Janda, *J. Chem. Phys.*, **92**, 5700 (1990).
16. J. J. Boland, *Phys. Rev. Lett.*, **67**, 1539 (1991).
17. J. J. Boland, *J. Vac. Sci. Technol. A*, **10**, 2458 (1992).
18. M. K. Farnaam and D. R. Olander, *Surf. Sci.*, **145**, 390 (1984).
19. W. L. M. Weerts, M. H. J. M. de Croon, and G. B. Marin, *Chem. Eng. Sci.*, **51**, 2109 (1996).
20. W. L. M. Weerts, M. H. J. M. de Croon, and G. B. Marin, *J. Electrochem. Soc.*, **144**, 3213 (1997).
21. C. R. Kleijn, Ph.D. Thesis, Delft University of Technology, Delft, The Netherlands (1991).
22. R. Becerra and R. Walsh, *J. Phys. Chem.*, **96**, 10856 (1992).
23. D. W. Marquardt, *J. Soc. Indust. Appl. Math.*, **11**, 431 (1963).
24. J. R. Kittrell, *Adv. Chem. Eng.*, **8**, 97 (1970).
25. N. R. Draper and H. Smith, *Applied Regression Analysis*, Wiley, New York (1966).
26. G. F. Froment and K. B. Bischoff, *Chemical Reactor Analysis and Design*, Wiley, New York (1990).
27. M. L. Hitchman, J. Kane, and A. E. Widmer, *Thin Solid Films*, **59**, 231 (1979).
28. J. Holleman and T. Aarnink, in *Chemical Vapor Deposition 1981*, J. M. Blocher, Jr., G. E. Vuillard, and G. Wahl, Editors, PV 81-7, p 307, The Electrochemical Society Proceedings Series, Pennington, NJ (1981).
29. R. F. C. Farrow, *J. Electrochem. Soc.*, **121**, 899 (1974).
30. R. C. Henderson and R. F. Helm, *Surf. Sci.*, **30**, 310 (1972).
31. M. J. Duchemin, M. M. Bonnet, and M. F. Koelsch, *J. Electrochem. Soc.*, **125**, 637 (1978).
32. R. J. Buss, P. Ho, W. G. Breiland, and M. E. Coltrin, *J. Appl. Phys.*, **63**, 2808 (1988).
33. D. J. Robbins and I. M. Young, *Appl. Phys. Lett.*, **50**, 1575 (1987).
34. D. W. Foster, A. J. Learn, and T. I. Kamins, *J. Vac. Sci. Technol. B*, **4**, 1182 (1986).
35. J. Holleman, Ph.D. Thesis, University of Twente, Enschede, The Netherlands (1993).
36. F. Hottier and R. Cadoret, *J. Cryst. Growth*, **52**, 199 (1981).
37. R. S. Rosler, *Solid State Technol.*, **20**, 63 (1977).
38. A. M. Beers and J. Bloem, *Appl. Phys. Lett.*, **41**, 153 (1982).
39. M. A. Ring and H. E. O'Neal, *J. Phys. Chem.*, **96**, 10848 (1992).
40. J. H. Purnell and R. Walsh, *Proc. R. Soc. London*, **A293**, 543 (1966).
41. R. T. White, R. L. Espino-Rios, D. S. Rogers, M. A. Ring, and H. E. O'Neal, *Int. J. Chem. Kinet.*, **17**, 1029 (1985).
42. G. Inoue, and M. Suzuki, *Chem. Phys. Lett.*, **122**, 361 (1985).
43. J. M. Jasinski, *J. Phys. Chem.*, **90**, 555 (1986).
44. J. M. Jasinski, *Mater. Res. Soc. Symp. Proc.*, **334**, 11 (1994).
45. J. M. Jasinski, R. Becerra, and R. Walsh, *Chem. Rev.*, **95**, 1203 (1995).
46. P. P. Gaspar, B.-H. Boo, and D. L. Svoboda, *J. Phys. Chem.*, **91**, 5011 (1987).
47. R. Becerra and R. Walsh, *J. Phys. Chem.*, **91**, 5765 (1987).
48. J. Dzarnoski, S. F. Rickborn, H. E. O'Neal, and M. A. Ring, *Organometallics*, **1**, 1217 (1982).
49. M. E. Coltrin, R. J. Kee, and G. H. Evans, *J. Electrochem. Soc.*, **136**, 819 (1989).
50. D. Burgess and M. R. Zachariah, *Mater. Res. Soc. Symp. Proc.*, **168**, 31 (1990).
51. M. E. Coltrin, R. J. Kee, and J. A. Miller, *J. Electrochem. Soc.*, **133**, 1206 (1986).
52. M. E. Coltrin, R. J. Kee, and J. A. Miller, *J. Electrochem. Soc.*, **131**, 425 (1984).
53. W. G. Breiland, M. E. Coltrin, and P. Ho, *J. Appl. Phys.*, **59**, 3267 (1986).
54. W. G. Breiland, P. Ho, and M. E. Coltrin, *J. Appl. Phys.*, **60**, 1505 (1986).
55. M. I. Temkin, *Int. Chem. Eng.*, **11**, 709 (1971).
56. H. N. Waltenburg and Y. T. Yates, *Surface Chemistry of Silicon*, Report (1994), Gov. Rep. Announce Index (U.S.), **95**, (1995), Abst. No. 17-00,554.
57. G. Schulze and M. Henzler, *Surf. Sci.*, **124**, 336 (1983).
58. B. G. Koehler, C. H. Mak, D. A. Arthur, P. A. Coon, and S. M. George, *J. Chem. Phys.*, **89**, 1709 (1988).
59. M. L. Wise, B. G. Koehler, P. Gupta, P. A. Coon, and S. M. George, *Surf. Sci.*, **258**, 166 (1991).
60. U. Höfer, L. Leping, and T. F. Heinz, *Phys. Rev. B.*, **45**, 9485 (1992).

61. D. J. Doren, in *Advances in Chemical Physics*, I. Prigogine and S. A. Rice, Editors, Vol. 95, p 1, John Wiley & Sons, New York (1996).
62. M. Boudart, *Kinetics of Chemical Processes*, Prentice-Hall, Englewood Cliffs, NJ (1968).
63. W. L. M. Weerts, M. H. J. M. de Croon, and G. B. Marin, *Surf. Sci.*, **367**, 321 (1996).
64. R. Imbihl, J. E. Demuth, S. M. Gates, and B. A. Scott, *Phys. Rev. B*, **39**, 5222 (1989).
65. K. J. Uram and U. Jansson, *Surf. Sci.*, **249**, 105 (1991).
66. S. K. Kulkarni, S. M. Gates, C. M. Greenlief, and H. H. Sawin, *Surf. Sci.*, **239**, 26 (1990).
67. S. K. Kulkarni, S. M. Gates, B. A. Scott, and H. H. Sawin, *Surf. Sci.*, **239**, 13 (1990).
68. P. Gupta, V. L. Colvin, and S. M. George, *Phys. Rev. B*, **37**, 8234 (1988).
69. M. Boudart and G. Djéga-Mariadassou, *Kinetics of Heterogeneous Catalytic Reactions*, Princeton University Press, Princeton, NJ (1984).
70. L. C. Feldman, P. J. Silverman, and I. Stensgaard, *Nucl. Instrum. Meth.*, **168**, 589 (1980).
71. K. J. Laidler, *Chemical Kinetics*, McGraw-Hill, New York (1973).
72. S. M. Gates, C. M. Greenlief, D. B. Beach, and R. R. Kunz, *Chem. Phys. Lett.*, **154**, 505 (1989).
73. S. M. Gates and S. K. Kulkarni, *Appl. Phys. Lett.*, **58**, 2963 (1991).
74. K. F. Roenigk, K. F. Jensen, and R. W. Carr, *J. Phys. Chem.*, **91**, 5732 (1987).
75. M. E. Coltrin, R. J. Kee, and G. H. Evans, *J. Electrochem. Soc.*, **136**, 819 (1989).
76. H. K. Moffat, K. F. Jensen, and R. W. Carr, *J. Phys. Chem.*, **96**, 7695 (1992).
77. J. M. Jasinski and J. O. Chu, *J. Chem. Phys.*, **88**, 1678 (1988).
78. A. Yeckel, S. Middleman, and A. K. Hochberg, *J. Electrochem. Soc.*, **136**, 2038 (1989).
79. B. S. Meyerson and W. Olbricht, *J. Electrochem. Soc.*, **131**, 2361 (1984).
80. F. C. Tompkins, *Chemisorption of Gases on Metals*, Academic Press, London (1978).
81. B. A. Scott, S. M. Gates, C. M. Greenlief, and R. D. Estes, in *Mechanisms of Reactions of Organometallic Compounds with Surfaces*, D. J. Cole-Hamilton and J. O. Williams, Editors, Vol. 97, Plenum Press, New York (1989).
82. R. Walsh, *Acc. Chem. Res.*, **14**, 246 (1981).
83. M. A. Vannice, S. H. Hyun, B. Kalpakci, and W. C. Liauh, *J. Catal.*, **56**, 358 (1979).
84. M. Boudart, D. E. Mears, and M. A. Vannice, *Ind. Chim. Belge*, **32**, 281 (1967).
85. D. H. Everett, *Trans. Faraday Soc.*, **46**, 957 (1950).

Temperature Dependence of the Electrical Properties of $SrBi_2Ta_2O_9$ Thin Films Deposited by Radio-Frequency Magnetron Sputtering

Cheol-Hoon Yang, Sang-Shik Park, and Soon-Gil Yoon*

Department of Materials Engineering, Chungnam National University, Daeduk Science Town, Taejon 305-764, Korea

ABSTRACT

Fatigue-free bilayered $SrBi_2Ta_2O_9$ (SBT) films were successfully prepared on Pt/Ti/SiO_2/Si substrates by radio-frequency magnetron sputtering. The applied voltage showing the maximum capacitance decreases with increasing temperature. The remanent polarization ($2P_r$) and the coercive field ($2E_c$) obtained for the SBT films were 13 $\mu C/cm^2$ and 128 kV/cm at an applied voltage of 5 V at 30°C. The films measured at room temperature and 100°C showed fatigue-free characteristics up to 10^{11} cycles under 5 V bipolar square pulses. SBT films show the retention loss of only 6% after 10 years at 100°C. The leakage current density is less than 4.5×10^{-7} $\mu A/cm^2$ at an applied voltage of 3 V at 75°C. The dominant transport mechanism of SBT films was an interface limited Schottky emission. The Pt/SBT contacts have a Schottky barrier height of $\Phi_B = 0.8 \sim 1.04$ eV.

Introduction

Recently, there has been great interest in the application of ferroelectric thin films in nonvolatile momories.[1-4] Lead-zirconate-titanate (PZT) or La modified lead-zirconate-titanate (PLZT) was initially considered to be the most promising candidate for nonvolitile memory application.[5] However, PZT or PLZT grown on Pt/Ti electrodes has poor polarization fatigue properties which afford only a limited number of switching cycles to the ferroelectric memories,[6-10] whereas strontium-bismuth-tantalate ($SrBi_2Ta_2O_9$) thin films have promising characteristics as a fatigue-free characteristic material for use in nonvolatile memory devices. The capacitors formed by bilayered $SrBi_2Ta_2O_9$ show no significant fatigue after 10^{12} switching cycles.[11,12] Ferroelectric capacitors need to meet many electrical requirements, including virtually unlimited endurance (more than 10^{12} read/write cycles) and good data retention (greater than 10 years) over a wide range of temperatures (0 to 70°C for consumer applications and −40 to 125°C for automotive applications). Capacitors involving an SBT ferroelectric layer have been synthesized mainly by metallorganic decomposition (MOD),[13,14] pulsed laser ablation (PLD),[15] and metallorganic chemical vapor deposition (MOCVD).[16] It is desirable to explore other techniques such as radio frequency (rf) magnetron sputtering.

In this work, the dependence of temperature on the electrical properties of sputtered SBT films was studied.

Experimental

Bilayered $SrBi_2Ta_2O_9$ (SBT) thin films were deposited on Pt(150 nm)/Ti(100 nm)/SiO_2(1,000 nm)/Si(100) substrates using a conventional rf magnetron sputtering technique. The targets were processed by mixing $SrCO_3$, Bi_2O_3, and Ta_2O_5 powders by ballmilling, calcinating the mixed powders at 1000°C, and then pressing the calcined powders into a 2 in. diam circular die. The composition of the targets was a $Sr_{1.2}Bi_{2.2}Ta_{2.0}O_9$ (SBT) ceramic with 20 and 20 mol % excess, $SrCO_3$ and Bi_2O_3 to compensate for the loss of Sr and Bi, respectively, in SBT films. The deposition of SBT films by rf magnetron sputtering was performed under a total pressure of 10 mTorr at 500°C. After pumping down the sputtering chamber to a base pressure of 5×10^{-6} Torr, argon and oxygen of 10 and 10 cm^3 min^{-1}, respectively, were introduced into the chamber using a mass flow controller. Oxygen was used to maintain the oxygen stoichiometry of the SBT films. The typical deposition conditions of SBT thin films are summarized in Table I.

* Electrochemical Society Active Member.